Chapter 16
Adaptive Observers for Structural Health Monitoring of High-Rate, Time-Varying Dynamic Systems

B. S. Joyce, J. Hong, J. C. Dodson, J. C. Wolfson, and S. Laflamme

Abstract Safe and reliable operation of hypersonic aircraft, space structures, advanced weapon systems, and other high-rate dynamic systems depends on advances in state estimators and damage detection algorithms. High-rate dynamic systems have rapidly changing input forces, rate-dependent and time-varying structural parameters, and uncertainties in material and structural properties. While current structural health monitoring (SHM) techniques can assess damage on the order of seconds to minutes, complex high-rate structures require SHM methods that detect, locate, and quantify damage or changes in the structure's configuration on the microsecond timescale.

This paper discusses the importance of microsecond structural health monitoring (μSHM) and some of the challenges that occur in development and implementation. Two model-based parameter estimators are examined for estimating the states and parameters of an example time-varying system consisting of a two degree of freedom system with a sudden change in a stiffness value that simulates structural damage. The ability of these estimators to track this stiffness change, the role of measurement noise, and the need for persistent excitation are examined.

Keywords Time-varying systems · Structural health monitoring · SHM · Damage detection · High-rate state estimation · Adaptive observer

16.1 Introduction

There are high-rate dynamic systems, such as hypersonic aircraft, space structures, and advanced weapon systems [1, 2], that experience uncertain and rapidly changing input forces, nonlinearities, time-varying structural parameters, and uncertainties in material and structural parameters. Due to the high rates of change in these systems, damage can quickly propagate through a structure and lead to severe loss of functionally [3, 4]. In order for damage prognosis and mitigation strategies to have enough time to react to a system change, structural health monitoring (SHM) that can detect, locate, and quantify system changes on microsecond timescales is needed.

Researchers are currently developing techniques for microsecond structural health monitoring (μSHM). Some methods under investigation utilize electromagnetic impedance-based methods to detect damage [5]. Other methods utilize adaptive neural-networks to describe the changing dynamics of a system before and after damage [6, 7]. These techniques are able to quickly detect changes in system configuration, but their data-driven nature makes it difficult to link changes in the measured response to a change in a specific system parameter. Therefore adaptive, model-based observers are needed to calculate system parameters and create a useful model for damage prognosis or feedback control schemes. Model-based techniques have been applied previously to civil structures for detecting damage [8–10], however parameter convergence rates in the microsecond to millisecond timescales have not yet been demonstrated with these methods.

B. S. Joyce (✉)
University of Dayton Research Institute (UDRI), Eglin AFB, FL, USA
e-mail: bryan.joyce@udri.udayton.edu

J. Hong
Applied Research Associates (ARA), Niceville, FL, USA

J. C. Dodson · J. C. Wolfson
Air Force Research Laboratory Fuzes Branch (AFRL/RWMF), Eglin AFB, FL, USA

S. Laflamme
Iowa State University, Ames, IA, USA

C. Niezrecki, J. Baqersad (eds.), *Structural Health Monitoring, Photogrammetry & DIC, Volume 6*,
Conference Proceedings of the Society for Experimental Mechanics Series, https://doi.org/10.1007/978-3-319-74476-6_16

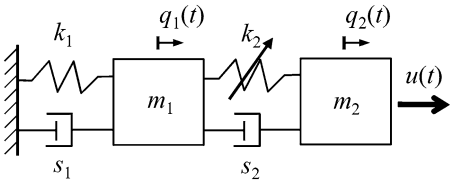

Fig. 16.1 Diagram of a two degree of freedom system with a changing stiffness k_2

This paper investigates the behavior of an example, time-varying system consisting of two masses connected by a spring and damper. The connecting spring undergoes a change in stiffness a few milliseconds into the simulation. Two parameter estimators are examined to estimate this stiffness. The first is a recursive least squares method with a forgetting factor that is based on full state feedback and knowledge of the mass and damping values. This estimator illustrates some of the challenges arising from these time-varying systems, such as the influence of noise, the tradeoff between robustness to noise and convergence speed, and the need for persistently exciting inputs. Next the system states and parameters are estimated using an extended Kalman filter with a forgetting factor. Simulation results show the benefits of using a forgetting factor and ensuring persistent excitation.

16.2 Example: Two Degree of Freedom System

An example system is created to demonstrate the issues that arise when estimating parameters in rapidly-changing system with noisy measurements. Consider the two degree of freedom system shown in Fig. 16.1. The system consists of two connected masses (m_1 and m_2) with displacements $q_1(t)$ and $q_2(t)$. The first mass is connected to a rigid ground with a stiffness k_1 and damper s_1. Connecting the two masses is a damper with a damping coefficient of s_2 and a spring with a time-varying spring stiffness of $k_2(t)$. An input force $u(t)$ is applied to the second mass. For the numerical simulations to follow, both mass are 1 kg, both damper coefficients are 0.1 N-s/m, and both stiffness values are initially 400 N/m. The stiffness of the connecting spring (k_2) is reduced by 5% to 380 N/m at 100 ms into the simulation. While the natural frequencies of this system before the stiffness change are low (1.97 Hz and 5.15 Hz), the results here could be scaled to higher frequency dynamics.

The equation of motion of this system can be written as

$$M\ddot{\mathbf{q}}(t) + S\dot{\mathbf{q}}(t) + K(t)\mathbf{q}(t) = \mathbf{\Gamma}_u u(t), \tag{16.1}$$

where the overdot denotes time differentiation, $\mathbf{q}$(t) is the vector of the displacements of the masses, M is the mass matrix, S is the damping matrix, $K(t)$ is the time-varying stiffness matrix, $\mathbf{\Gamma}_u$ is the force influence vector, and $u(t)$ is the input force. The above vectors and matrices are defined as

$$\mathbf{q}(t) = \begin{bmatrix} q_1(t) \\ q_2(t) \end{bmatrix}, \mathbf{\Gamma}_u = \begin{bmatrix} 0 \\ 1 \end{bmatrix}, \tag{16.2}$$

$$M = \begin{bmatrix} m_1 & 0 \\ 0 & m_2 \end{bmatrix}, S = \begin{bmatrix} s_1 + s_2 & -s_2 \\ -s_2 & s_2 \end{bmatrix}, K(t) = \begin{bmatrix} k_1 + k_2(t) & -k_2(t) \\ -k_2(t) & k_2(t) \end{bmatrix}. \tag{16.3}$$

In state space form, Eq. (16.1) can be written as

$$\dot{\mathbf{x}}(t) = A(t)\mathbf{x}(t) + \mathbf{B}u(t), \tag{16.4}$$

where $\mathbf{x}(t)$ is the state vector, $A(t)$ is the state matrix, and $\mathbf{B}$ is the input matrix defined as

$$\mathbf{x}(t) = \begin{bmatrix} \mathbf{q}(t) \\ \dot{\mathbf{q}}(t) \end{bmatrix}, A(t) = \begin{bmatrix} 0 & I \\ -M^{-1}K(t) & -M^{-1}S \end{bmatrix}, \mathbf{B} = \begin{bmatrix} 0 \\ M^{-1}\mathbf{\Gamma}_u \end{bmatrix}. \tag{16.5}$$

In general, measurements from this system, $\mathbf{y}(t)$, can be written as

$$\mathbf{y}(t) = C(t)\mathbf{x}(t) + \mathbf{D}u(t). \tag{16.6}$$

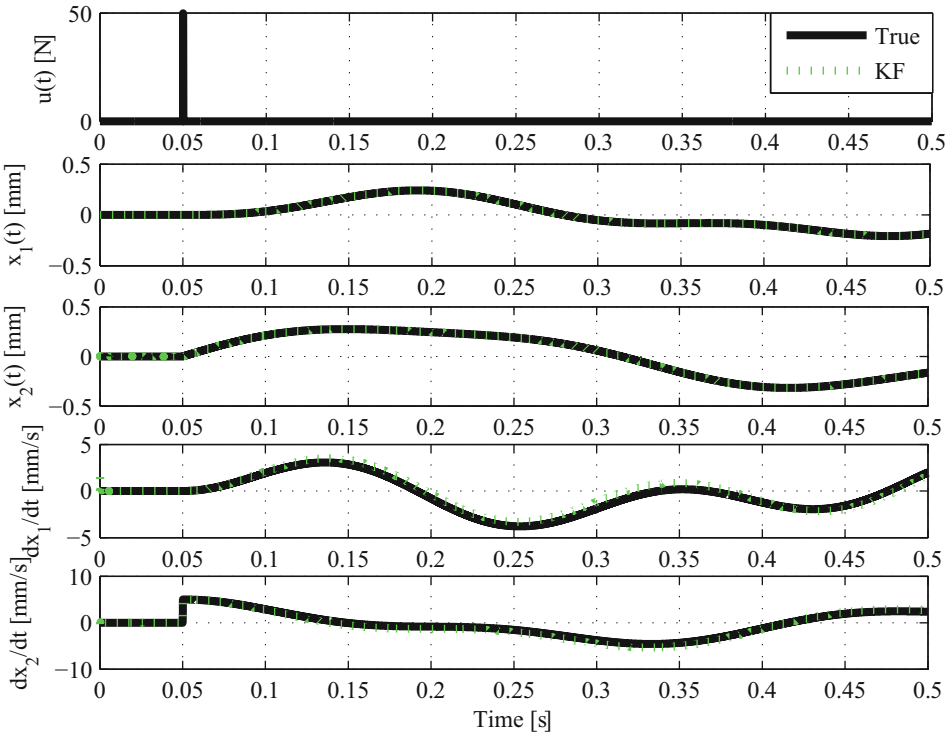

Fig. 16.2 Response of the example two degree of freedom system to an impulse at time 50 ms and a 5% change in stiffness k_2 at 100 ms. The legend in the top plot applies to all lines in this figure. From comparison, estimated states from a standard Kalman filter (KF) are also shown

where $C(t)$ is the output matrix and $\mathbf{D}$ is the direct feedthrough matrix. If the displacements of both masses are measured, then $\mathbf{y}(t)$, $C(t)$, and $\mathbf{D}$ are

$$\mathbf{y}(t) = \mathbf{q}(t), C(t) = [I \ \ 0], \mathbf{D} = \mathbf{0}, \tag{16.7}$$

where the identity matrix I, the zero matrix 0, and the zero vector $\mathbf{0}$ have the appropriate sizes. For velocity measurements from both masses, these take the forms

$$\mathbf{y}(t) = \dot{\mathbf{q}}(t), C(t) = \begin{bmatrix} 0 \ I \end{bmatrix}, \mathbf{D} = \mathbf{0}, \tag{16.8}$$

For acceleration measurements from both masses, these are written as

$$\mathbf{y}(t) = \ddot{\mathbf{q}}(t), C(t) = \begin{bmatrix} -M^{-1}K(t) \ -M^{-1}S \end{bmatrix}, \mathbf{D} = M^{-1}\mathbf{\Gamma}_u. \tag{16.9}$$

These three different measurement cases (displacements, velocities, or accelerations for both masses) will be considered in the results that follow.

Figure 16.2 shows the response of the two degree of freedom subject to an impulse of amplitude 50 N at 50 ms and a 5% reduction in the connecting spring stiffness k_2 at 100 ms. The simulation sampling rate is 50 kHz. This true system response is plotted beside estimated state values from a standard Kalman filter (KF) with displacement measurements. Here noise is added such that the signal-to-noise ratio for each measured displacement is 60 dB. The observers are given a 10% initial error for k_2 (440 N/m) that remains unchanged over the duration of the simulation. All other parameters in the estimators are their true values. This discrepancy between the true value of k_2 and that used by the state observers results in some error in velocity, but the errors are small over this time interval. Therefore, deviations between the true states and those from a fixed-parameter observer may not be sufficient to detect system damage.

16.3 Methods

To illustrate some of the challenges that arise in high-rate parameter estimation, the stiffness values k_1 and k_2 at each time step are estimated through two methods. The first is a recursive least squares (RLS) method with a forgetting factor. The second is an extended Kalman filter with a forgetting factor. The role of the forgetting factor and other issues faced by these estimators will be discussed in the simulation results that follow.

16.3.1 Recursive Least Squares

First the recursive least squares approach is used to estimate the unknown stiffness values of the two springs in the example system. Here it is assumed that the input force and the displacements, velocities, and accelerations of the two masses are measured, and it is assumed the masses (m_1 and m_2) and damper coefficients (s_1 and s_2) are known. This set of information can be used to derive a recursive least squares estimation of the two stiffness values k_1 and k_2. While difficult to implement directly in practice, this method illustrates the role of state or measurement uncertainties on the estimated parameters and can help tune settings in other adaptive state and parameter estimators.

First, rewrite the equation of motion, Eq. (16.1), as

$$K(t)\mathbf{q}(t) = \mathbf{\Gamma}_u u(t) - M\ddot{\mathbf{q}}(t) + S\dot{\mathbf{q}}(t). \tag{16.10}$$

This can be re-written as a least squares problem of the form

$$\varphi(t)\boldsymbol{\theta}(t) = \mathbf{T}(t), \tag{16.11}$$

where the parameter vector $\boldsymbol{\theta}$ and the other matrices and vectors are defined as

$$\boldsymbol{\theta}(t) = \begin{bmatrix} k_1(t) \\ k_2(t) \end{bmatrix}, \varphi(t) = \begin{bmatrix} q_1(t) & q_1(t) - q_2(t) \\ 0 & q_2(t) - q_1(t) \end{bmatrix}, \text{and } \mathbf{T}(t) = \mathbf{\Gamma}_u u(t) - M\ddot{\mathbf{q}}(t) + S\dot{\mathbf{q}}(t) \tag{16.12}$$

This can be solved using a recursive least squares method (RLS) with an exponential forgetting factor λ. See for example [11]. This algorithm is summarized in Fig. 16.3 below. Here the equations above are written in discrete time with time index k. The forgetting factor λ is a value between 0 and 1 and serves to weight previous data with less importance. Smaller forgetting factors mean that current samples are given more importance over older data. This means that smaller forgetting factors reduce estimation time but make the estimator less robustness to measurement noise.

16.3.2 Extended Kalman Filter

Another method of parameter estimation is the extended Kalman filter. Here a joint extended Kalman filter is used whereby the unknown model parameters are treated as additional states. In this case, the dynamic equations can be written as

Initialize estimated parameters $\hat{\boldsymbol{\theta}}_0$ and error covariance matrix P_0

for $k = 1{:}N$

Assemble φ_k and $\mathbf{T}_k$ as defined in equations (12)

Calculate the Kalman gain: $L_k = P_{k-1}\varphi_k\left[\lambda I + \varphi_k^T P_{k-1}\varphi_k\right]^{-1}$

Update the parameter estimate: $\hat{\boldsymbol{\theta}}_k = \hat{\boldsymbol{\theta}}_{k-1} + L_k\left[\mathbf{T}_k - \varphi_k^T\hat{\boldsymbol{\theta}}_{k-1}\right]$

Update the error covariance estimate: $P_k = \left[I - L_k\varphi_k^T\right]\lambda^{-1}P_{k-1}$

end

Fig. 16.3 Algorithm for the recursive least squares (RLS) with a forgetting factor λ

$$\begin{bmatrix} \dot{\mathbf{x}}(t) \\ \dot{\boldsymbol{\theta}}(t) \end{bmatrix} = \begin{bmatrix} A\left(\boldsymbol{\theta}(t)\right)\mathbf{x}(t) + \mathbf{B}u(t) \\ \mathbf{0} \end{bmatrix}, \tag{16.13}$$

$$\mathbf{y}(t) = C\left(\boldsymbol{\theta}(t)\right)\mathbf{x}(t) + \mathbf{D}u(t). \tag{16.14}$$

For implementation, these continuous time equations will need to be discretized. One method for doing this is to use an Euler approximation for the derivative. This gives

$$\begin{bmatrix} \mathbf{x}_k \\ \boldsymbol{\theta}_k \end{bmatrix} = \begin{bmatrix} \left(I + \Delta t A\left(\boldsymbol{\theta}_{k-1}\right)\right)\mathbf{x}_{k-1} + \Delta t\, \mathbf{B}u_{k-1} \\ \boldsymbol{\theta}_{k-1} \end{bmatrix} + \mathbf{w}_k, \tag{16.15}$$

$$\mathbf{y}_k = C\left(\boldsymbol{\theta}_k\right)\mathbf{x}_k + \mathbf{D}u_k + \mathbf{v}_k, \tag{16.16}$$

where the subscript k is the time index and Δt is the time between samples. In Eqs. (16.17) and (16.18), process and measurement noise are also introduced. The process noise $\mathbf{w}_k$ is assumed Gaussian with zero mean and a covariance $\mathbf{Q}$, and the measurement noise $\mathbf{v}_k$ is also assumed to be Gaussian with zero mean and a covariance $\mathbf{R}$. Next, define the augmented state vector $\mathbf{x}^a$ as the concatenation of the state and parameter vectors, i.e.

$$\mathbf{x}_k^a = \begin{bmatrix} \mathbf{x}_k \\ \boldsymbol{\theta}_k \end{bmatrix}. \tag{16.17}$$

From this, Eqs. (16.15) and (16.16) take the general form

$$\mathbf{x}_k^a = \mathbf{f}\left(k, \mathbf{x}_{k-1}^a, u_{k-1}\right) + \mathbf{w}_k, \tag{16.18}$$

$$\mathbf{y}_k = \mathbf{h}\left(k, \mathbf{x}_k^a, u_k\right) + \mathbf{v}_k. \tag{16.19}$$

From this point, these equations are implemented in an extended Kalman filter (EKF) algorithm. Here the standard EKF algorithm is modified to include a forgetting factor like that of the previous RLS estimator. Figure 16.4 below lists the algorithm for the EKF with forgetting factor. The algorithm is similar to that used by Yang [9] or Xia [12] but with a constant forgetting factor λ. In Fig. 16.4, the subscript "$k|k$-1" denotes predictions of the augmented state vector or the error covariance matrix at time k based on previous data. The procedure is like that of a standard EKF algorithm, but the introduction of the forgetting factor λ has the effect of weighing the previous estimated states with less importance.

16.3.3 Persistent Excitation

Successful parameter convergence depends on having persistently exciting input and measurement signals in order for parameters to converge to a unique solution [11]. One method of quantifying the degree of persistent excitation is to define a persistent excitation metric ρ as

$$\rho(t) = \left\|\varphi(t)\varphi^T(t)\right\|, \tag{16.20}$$

where the matrix 2-norm is used (equivalent to the largest singular value of the matrix), and $\varphi(t)$ is defined in Eq. (16.12). If ρ is close to zero, the RLS algorithm will result in poor parameter estimates due to numerical instabilities.

There are a few methods to overcome this persistent excitation problem. The first is to modify the update law to not estimate states during periods of small measurements. In this approach, if the initial estimates of the parameters are incorrect, then the estimator cannot adjust them to their correct values until a sufficiently large excitation is delivered. This will lead to overall longer converge times. Instead, consider adding an additional, small amplitude forcing term to the original force, i.e. let the input $u(t)$ be

$$u(t) = F\delta\left(t - t_0\right) + \eta(t). \tag{16.21}$$

Initialize estimated augmented state $\hat{\mathbf{x}}_0^a$ and error covariance P_0

for $k = 1{:}N$

Calculate the Jacobians $\hat{A}_k = \left[\frac{\partial \mathbf{f}}{\partial \mathbf{x}^a}\right]_{\mathbf{x}^a=\mathbf{x}_k^a,\mathbf{u}=\mathbf{u}_k}$ and $\hat{C}_k = \left[\frac{\partial \mathbf{h}}{\partial \mathbf{x}^a}\right]_{\mathbf{x}^a=\mathbf{x}_k^a,\mathbf{u}=\mathbf{u}_k}$

Predict state at k: $\hat{\mathbf{x}}_{k|k-1}^a = \mathbf{f}\left(k, \hat{\mathbf{x}}_{k-1}^a, \mathbf{u}_{k-1}\right)$

Predict state error covariance at k: $P_{k|k-1} = \lambda^{-1}\hat{A}_k\ P_{k-1}\ \hat{A}_k^T + Q$

Calculate the Kalman gain: $L_k = P_{k|k-1}\hat{C}_k^T\left(\hat{C}_k P_{k|k-1}\hat{C}_k^T + R\right)^{-1}$

Estimate output: $\hat{\mathbf{y}}_k = \mathbf{h}\left(k, \hat{\mathbf{x}}_{k|k-1}^a, u_k\right)$

Update augmented state estimate: $\hat{\mathbf{x}}_k^a = \hat{\mathbf{x}}_{k|k-1}^a + L_k\left(\mathbf{y}_k - \hat{\mathbf{y}}_k\right)$

Update error covariance: $P_k = \left(I - L_k\hat{C}_k\right)P_{k|k-1}\left(I - L_k\hat{C}_k\right)^T + L_k\ R\ L_k^T$

end

Fig. 16.4 Algorithm for the extended Kalman filter (EKF) with a forgetting factor λ

where F is the amplitude of the impulse, t_0 is the time of the impulse, and $\eta(t)$ is an additional, zero-mean, stochastic force that may be broadband or filtered to a specified frequency band. This additional force excites the system at all times. This allows the estimator to converge to the correct parameter values before the impulse occurs. This is important in many applications where the parameters of the as-built system need to be determined before the system is used in operation. The benefit of this additional force will be demonstrated in the simulation results that follow.

16.3.4 Metrics for Performance Comparison

The performance of the estimators before damage (drop in stiffness value) and after damage can be compared numerically in terms of the settling time and the normalized root-mean-square error (NRMSE). The settling time is taken as the time it takes the stiffness estimate to settle within ± 1 N/m of the true, final stiffness value. Smaller settling times correspond to a faster parameter convergence. The NRMSE is defined as the ratio between the root-mean-square (RMS) value of the error and the RMS value of the true parameter, i.e.

$$NRMSE = \frac{\sqrt{\frac{1}{N}\sum_{k=1}^{N}\left(\widehat{\theta}_k - \theta_k\right)^2}}{\sqrt{\frac{1}{N}\sum_{k=1}^{N}(\theta_k)^2}}, \tag{16.22}$$

where N is the number of points in time considered in the calculation.

16.4 Simulation Results

16.4.1 Recursive Least Squares

First consider the results from the RLS method. Figure 16.5 shows the stiffness estimation results for different forgetting factors (λ). The simulation conditions are the same as those used to generate Fig. 16.2. For the RLS estimator, noise is added to each signal (displacements, velocities, accelerations, and input) such that each has a specified signal-to-noise ratio

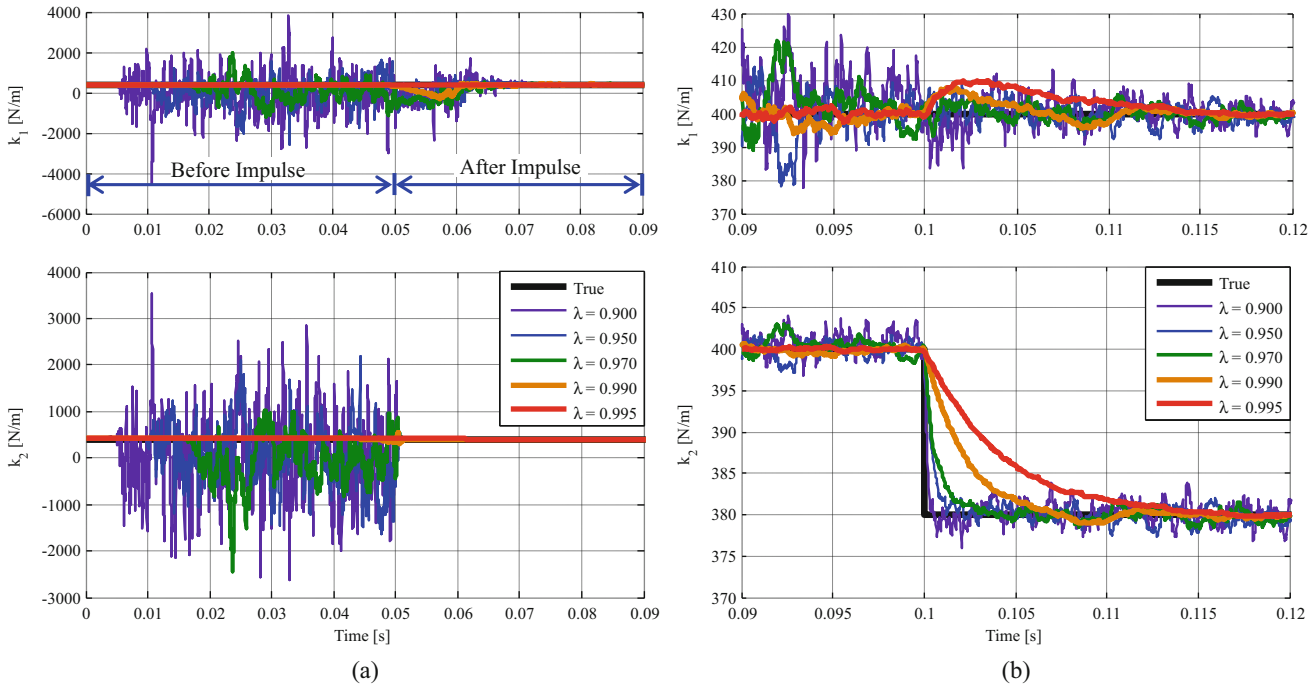

Fig. 16.5 Estimated spring stiffness values for varying values of λ at a fixed 60 dB signal-to-noise ratio on each state and input value. (**a**) Estimations before and after the initial impulse at 0.05 s (50 ms). (**b**) Estimations around the 5% stiffness change at 0.1 s (100 ms)

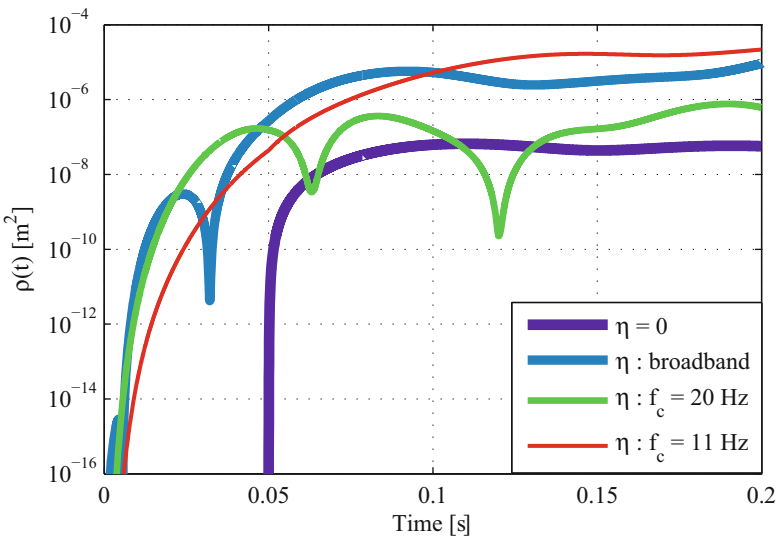

Fig. 16.6 Persistent excitation metric $\rho(t)$ based on the noise-free displacements. The baseline, impulse only condition is shown ($\eta = 0$) alongside using an additional stochastic noise term that is broadband to 25 kHz or filtered at a corner frequency (f_c) of 20 Hz and 11 Hz

of 60 dB. The estimator is given a 10% initial error for k_2 of 440 N/m instead of the correct initial stiffness of 400 N/m. Only measurement noise is provided to the algorithms before the impact at 50 ms, and therefore the stiffness estimates are initially poor in all cases. This lack of excitation can also be illustrated in the persistent excitation metric $\rho(t)$ shown in Fig. 16.6. Before the impulse at 50 ms, the displacements are zero and therefore ρ is zero (the $\eta = 0$ case in Fig. 16.6). When there is not sufficient dynamics to overcome the measurement noise, larger estimation errors can arise. When the system begins to respond with sufficient amplitude, the estimators must now converge to the correct parameter values from the initial large estimation errors. When system motion ceases, this problem will arise again. This initial error can be reduced and overall robustness to noise can be increased by increasing the forgetting factor λ closer to 1. However, increasing λ produces a slower update rate and reduces the time to parameter convergence.

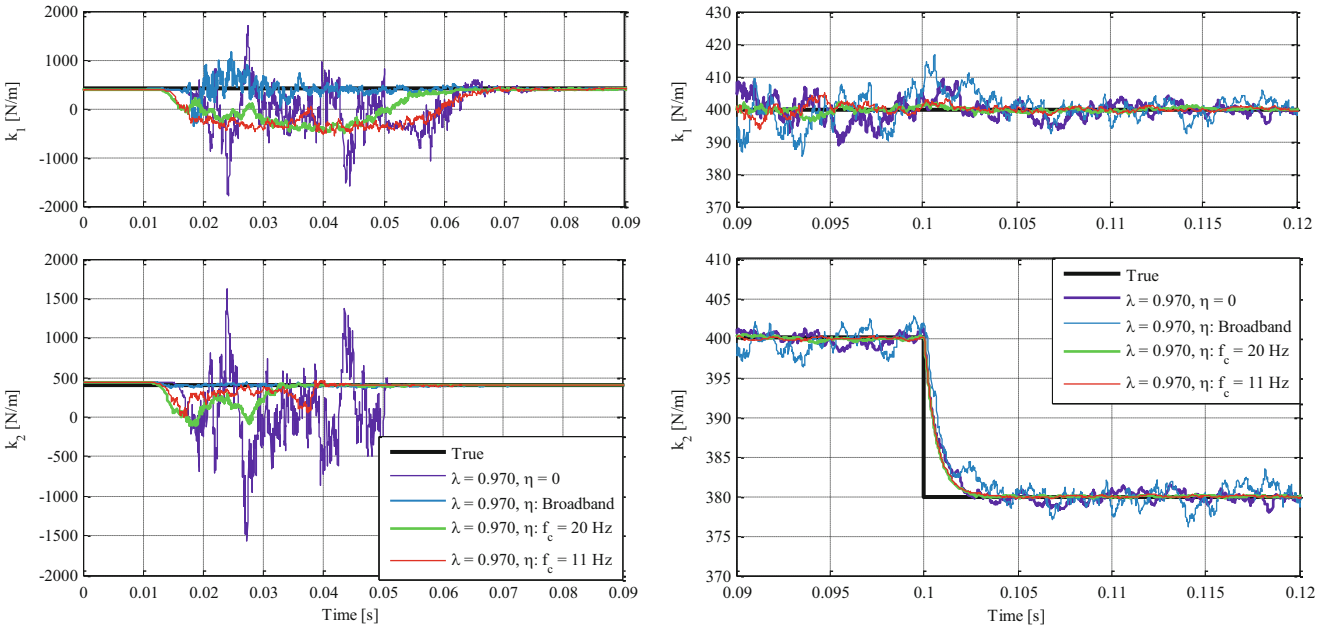

Fig. 16.7 Estimation results from the recursive least squares (RLS) estimator for varying additional inputs $\eta(t)$. (**a**) Estimations before and after the initial impulse. (**b**) Estimations during the 5% stiffness change. For all cases the forgetting factor is set to 0.970

Consider now adding an additional, stochastic input force $\eta(t)$ as in Eq. (16.21). Figure 16.6 shows the persistent excitation condition for different cases of $\eta(t)$ including broadband, Gaussian-distributed excitation to half the simulation's sampling rate (25 kHz), that excitation filtered with a low-pass filter of corner frequency 20 Hz, and the excitation filtered to 11 Hz. In all cases, $\eta(t)$ is given unit variance. All three added input forces create an improvement in the initial persistent excitation metric $\rho(t)$. The benefit of this increase initial excitation can be seen in the simulation results in Fig. 16.7. Initially the addition of a broadband η gives better robustness in the stiffness estimates than the impulse alone, but this broadband excitation causes more oscillations in the response later in the simulation during the parameter change. Filtering η results in slower initial convergence but better tracking during the stiffness change.

Figure 16.8 shows the NRMSE and the settling time for the connecting stiffness k_2 estimate using the recursive least squares (RLS) estimator. Results are shown with the additional force term set to zero ("$\eta = 0$" in the figure) and with added white noise filtered at 20 Hz ("η: $f_c = 20$ Hz" in the figure). The errors and settling times are considered before damage and after damage. Because of the random measurement noise and stochastic forcing terms in the simulations, NRMSE and settling times are averaged over five repetitions of the simulations at each condition. Error bars on the plots indicate two standard deviations above and below the mean.

In general, the additional force η reduces the NRMSE and the settling time. This extra force greatly reduces the error before damage occurs when there is 50 ms before the impact when the measurements would otherwise be only noise. This stochastic force introduces more variability in all of the simulation results. This variability in NRMSE decreases with increasing forgetting factors.

Larger forgetting factors generally decrease the NRMSE by making the estimates less influenced by noise. Before damage, the forgetting factor has little influence on the settling time during this initial period of high errors. After damage, there is only a noticeable increase in settling time for the 0.995 forgetting factor case. While none of the settling times in these examples are on the order of microseconds, these results do illustrate that adjusting the forgetting factor and introducing an additional force term can decrease parameter convergence times.

16.4.2 Extended Kalman Filter

Figure 16.9 shows the simulation results from the extended Kalman filter for the impulse only ($\eta = 0$) and with the additional stochastic force $\eta(t)$ filtered at 20 Hz. Here displacement measurements are used with a signal-to-noise ratio of 60 dB. The

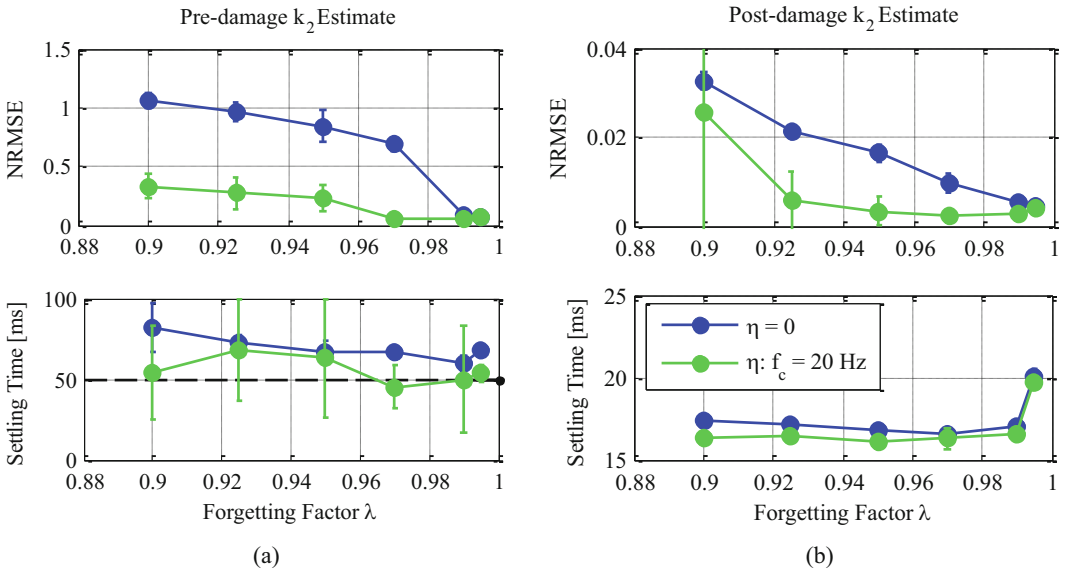

Fig. 16.8 Comparisons of the normalized root-mean-square error (NRMSE) and settling time for estimating the changing stiffness k_2 using the recursive least squares (RLS) estimator. (**a**) NRMSE and settling time before damage occurs. (**b**) NRMSE and settling time after damage. The legend in (**b**) applies to both (**a**) and (**b**)

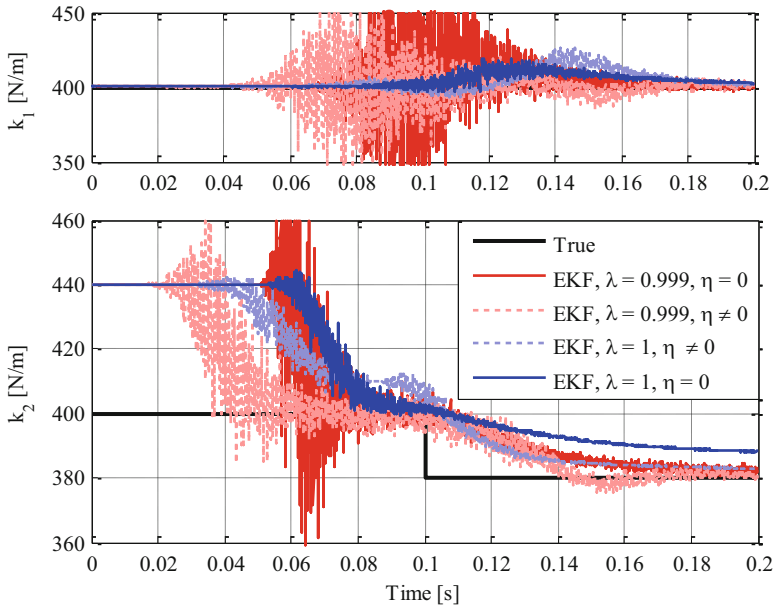

Fig. 16.9 Estimates of the stiffness values for the example system using the extended Kalman filter for different forgetting factors λ and with and without the additional stochastic force $\eta(t)$

standard extended Kalman filter is shown ($\lambda = 1$) beside one with a forgetting factor ($\lambda = 0.999$). Introducing $\eta(t)$ to the input reduces the initial convergence time both with and without the forgetting factor. The use of a forgetting factor improves overall convergence rate, but reduces the robustness to noise.

Table 16.1 lists the NRMSE for the EKF estimate of k_2, and Table 16.2 lists the settling time for the EKF estimate. The results compare the EKF with and without the stochastic force term filtered to 20 Hz. Note that the stiffness estimate does not settle within 1 N/m of the correct value before damage. Note also that the stiffness does not converge during the simulation time without the stochastic noise term and a forgetting factor of 1. As with the RLS method, the use of the additional force term reduces the NRMSE before damage during the initial parameter convergence. After damage occurs, the additional force term improves the average convergence times but introduces a large amount of variability in the settling time estimate. This

Table 16.1 Normalized root-mean-square error (NRMSE) for the EKF estimate of k_2 for the different conditions shown in Fig. 16.9 before and after damage. Two standard deviations above and below the mean are also listed. Note that the deviation in the simulation results is negligible when no stochastic force term is present

	Before damage		After damage	
	$\eta = 0$	$\eta \neq 0$	$\eta = 0$	$\eta \neq 0$
$\lambda = 0.999$	8.1%	(7.4 ± 1.3) %	1.3%	(1.1 ± 0.4) %
$\lambda = 1.000$	8.3%	(8.1 ± 2.1) %	2.2%	(2.0 ± 1.2) %

Table 16.2 Settling time for the EKF estimate of k_2 for the different conditions shown in Fig. 16.9 after damage. Two standard deviations above and below the mean are also listed. Note that the stiffness estimate does not settle to within the specified limit before damage occurs

	$\eta = 0$	η: $f_c = 20$ Hz
$\lambda = 0.999$	200 ± 2 ms	130 ± 80 ms
$\lambda = 1.000$	(Does not converge)	630 ± 360 ms

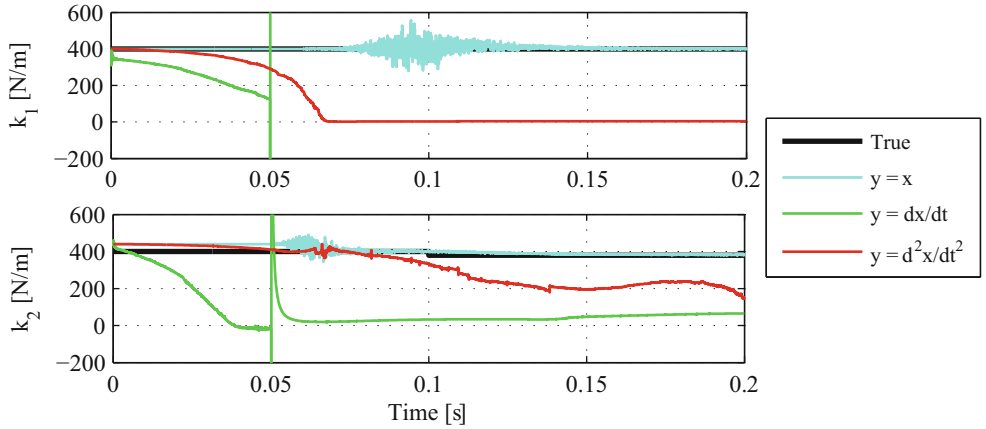

Fig. 16.10 Estimated stiffness values from the extended Kalman filter (EKF) using displacement (x), velocity (dx/dt), or acceleration (d^2x/dt^2) measurements. The forgetting factors λ is 0.999 and no additional stochastic force $\eta(t)$ is used

indicates that it may be useful to switch off the additional force term after a sufficiently large input force is applied to the system. Both NRMSE and convergence times are improved by using a forgetting factor. Note that the convergence times here are about one order of magnitude longer than those seen in the RLS method.

Finally, while results using displacement feedback to the observers show parameter convergence, the results are worse when using other types of measurements. Figure 16.10 shows the results using displacement, velocity, and acceleration measurements. The inability of the algorithm to converge illustrates that the type of measurement can have a role in the stability and observability of parameter estimates.

16.5 Conclusions and Future Work

There is a need for high rate state and parameter estimators for structural health monitoring and feedback control of complex systems. This paper illustrated some of the issues that are encountered in high rate parameter estimation and discussed methods of comparing and quantifying parameter error and convergence rates. A recursive least squares (RLS) estimator and an extended Kalman filter (EKF) were examined for estimating the stiffness values for an example, two degree of freedom system. Simulation results using a RLS technique illustrated the benefits of using a forgetting factor and ensuring persistent excitation. The forgetting factor allowed the estimator to more quickly adapt to parameter changes but at the expense of making the estimations more sensitive to measurement noise. Adding an additional, low-amplitude force term increased the initial persistent excitation metric and led to overall faster convergence times. Introducing forces on a structure before an external impact could allow the estimators to initially converge to the proper system parameters before damage occurs. It should also be noted that while only k_2 changed, the estimator may change both stiffness values in order to find the best parameters that solve the least squares problem in Eq. (16.11) as seen in Fig. 16.5. Care must be taken to ensure

this does not indicate a false state of damage in a structural health monitoring algorithm. Results from the EKF show the same benefits of a forgetting factor and an additional, persistent force term. The EKF results also show that the type of measurement (displacement, velocity, or acceleration) influenced the stability of parameter estimators with the displacement measurements providing the most accurate estimates.

The work presented here motivates the need to develop robust, adaptive observers with rapid state and parameter convergence. Future work will examine developing new, adaptive observers that incorporate forgetting factors and added stochastic input forces to reduce convergence times. In addition there is a need to examine the state and parameter observability of these systems to select the measurement locations and measurement types to best estimate particular system parameters. Simulation results here considered a two degree of freedom system with low natural frequencies. Future work will also consider the role of higher system natural frequencies and faster system dynamics on the ability of these estimators to track state and parameter changes.

Acknowledgements This material is based upon work supported by the Air Force Office of Scientific Research under award numbers FA9550-17RWCOR503 and FA9550-17-1-0131. Any opinions, findings, and conclusions or recommendations expressed in this material are those of the authors and do not necessarily reflect the views of the United States Air Force. Distribution A. Approved for public release; distribution unlimited (96TW-2017-0440).

References

1. Stein, C., Roybal, R., Tlomak, P., Wilson, W.: A review of hypervelocity debris testing at the Air Force Research Laboratory. Space Debris. **2**(4), 331–356 (2000). https://doi.org/10.1023/B:SDEB.0000030024.23336.f5
2. Hallion, R.P., Bedke, C.M., Schanz, M.V.: Hypersonic Weapons and US National Security, a 21st Century Breakthrough. Mitchell Institute for Aerospace Studies, Air Force Association, Arlington (2016)
3. Dodson, J., Inman, D.J., Foley, J.R.: Microsecond structural health montoring in impact loaded structures. In: Proc. Proceedings in SPIE, San Diego
4. Lowe, R., Dodson, J., Foley, J.: Microsecond prognostics and health monitoring. IEEE Reliability Society Newsletter. **60**, 1–5 (2014)
5. Kettle, R., Dick, A., Dodson, J., Foley, J., Anton, S.R.: Real-time detection in highly dynamic systems. In: Proc. IMAC XXXIV A Conference and Exposition on Structural Dynamics, Orlando
6. Hong, J., Laflamme, S., Cao, L., Dodson, J.: Variable input observer for structural health monitoring of high-rate systems. In: Proc. AIP Conference Proceedings, p. 07003
7. Hong, J., Laflamme, S., Dodson, J.: Variable input spce observer for structural health monitoring of high-rate system. In: Proc. Review of Progress in Quantitative Nondestructive Evaluation (QNDE)
8. Doebling, S., Farrar, C.R., Prime, M.B.: A summary review of vibration-based damage identification methods. Shock Vib. Dig. **30**, 91–105 (1998). https://doi.org/10.1177/058310249803000201
9. Yang, J.N., Lin, S., Huang, H., Zhou, L.: An adaptive extended Kalman filter for structural damage identification. Struct. Control. Health Monit. **13**(4), 849–867 (2006). https://doi.org/10.1002/stc.84
10. Yang, J.N., Pan, S., Huang, H.: An adaptive extended Kalman filter for structural damage identifications II: unknown inputs. Struct. Control. Health Monit. **14**(3), 497–521 (2007). https://doi.org/10.1002/stc.171
11. Åström, K.J., Witternmark, B.: Adaptive Control. Addison-Wesley Longman Publishing Co., Inc., Boston (1994)
12. Xia, Q., Roa, M., Ying, Y., Shen, X.: Adaptive fading Kalman filter with an application. Automatica. **30**(8), 1333–1338 (1994). https://doi.org/10.1016/0005-1098(94)90112-0